Journal of The Electrochemical Society, **150** (1) A98-A106 (2003)
0013-4651/2003/150(1)/A98/9/$7.00 © The Electrochemical Society, Inc.

Analysis of Electrochemical and Thermal Behavior of Li-Ion Cells

Venkat Srinivasan* and C. Y. Wang,z**

Electrochemical Engine Center, and Departments of Mechanical Engineering and Materials Science and Engineering, The Pennsylvania State University, University Park, Pennsylvania 16802, USA

This paper seeks to gain a better understanding of the thermal behavior of Li-ion cells using a previously developed two-dimensional, first principles-based thermal-electrochemical modeling approach. The model incorporates the reversible, irreversible, and ohmic heats in the matrix and solution phases, and the temperature dependence of the various transport, kinetic, and mass-transfer parameters based on Arrhenius expressions. Experimental data on the entropic contribution for the manganese oxide spinal and carbon electrodes, recently published in the literature, are also incorporated into the model in order to gauge the importance of this term in the overall heat generation. Simulations were used to estimate the thermal and electrical energy and the active material utilization at various rates in order to understand the effect of temperature on the electrochemistry and vice versa. In addition, the methodology of using experimental data, instead of an electrochemical model, to determine the heat-generation rate is examined by considering the differences between the local and lumped thermal models, and the assumption of using heat generation rate determined at a particular thermal environment under other conditions. Model simulations are used to gain insight into the appropriateness of various approximations in developing comprehensive thermal models for Li-ion cells.
 [DOI: 10.1149/1.1526512]

Manuscript submitted March 18, 2002; revised manuscript received July 12, 2002. Available electronically December 3, 2002.

Dual-lithium insertion cells have gained prominence in recent years because of their superior energy and power densities compared to the presently used Ni-metal hydride (MH) cells. These cells, while presently used largely in laptop and cell phone applications, are expected to replace Ni-MH and lead-acid cells in electric and hybrid electric vehicles in the near future. This promising market has spurred research into this battery chemistry with emphasis ranging from material development, with the aim of improving cycle life and capacity, to cell design to maximize the energy and power density. While many of these issues have been solved, one major concern in these cells is thermal runaway, with the ensuing property hazard and safety issues. Considerable research has therefore been undertaken to understand the thermal behavior of Li-ion cells with the aim of being able to anticipate thermal runaway. This understanding has been forged using experimental observations, where data on heat generation is collected during charge/discharge[1-3] and/or by studying the self-heating of the cells using accelerating rate calorimeter (ARC)-type experiments.[4] In addition, fundamental properties, like the entropy of the intercalation reaction as a function of state-of-charge (SOC), have also been measured.[5,6]

Simultaneously, various mathematical models for the system have been developed in order to complement the experimental measurements. Models that either address a single cell[7-11] or cell stacks[1,12,13] have been developed where a thermal model is coupled with either a first principles electrochemical model or experimental data to account for the heat generation. Pals and Newman[10,13] developed a thermal model for a Li-ion cell by building on the electrochemical model presented by Doyle *et al.*[14] and study the discharge of a single cell[10] and extend it to that of a cell stack.[13] In order to reduce the complexity, they used the global energy balance method presented by Bernardi *et al.*[15] to describe a single cell and use the heat generation estimated by isothermal discharge to simulate a stack. The authors point out that the isothermal assumption is inexact and show the magnitude of the error when simulating cell stacks. However, no attempt was made to quantify this effect as a function of rate. This global energy balance approach has also been used by Botte *et al.*,[8] who simulated the thermal behavior of a Li-ion cell by incorporating the decomposition of the carbon electrode, and by Baker and Verbrugge[7] to simulate the behavior of thin-film batteries under various conditions. In addition, Song and Evans[12] take a similar approach and present a 2D thermal model for a cell stack where the heat generation is estimated from a 1D electrochemical model. In other words, it is assumed that concentrations, current, and overpotential variations across the cell height are negligible.

While the above papers take the global energy balance approach presented by Bernardi *et al.*,[15] Rao and Newman[11] show the importance of incorporating the local differences in the reaction current and SOC in estimating the true heat generation in the cell. The authors show that the previously used approach was an approximation valid only when the reaction distribution was uniform in the cell. The nature of the open-circuit potential (OCP) *vs.* SOC curve was seen to be important in deciding the differences. Based on this knowledge, Gu and Wang[9] presented a 2D thermal-electrochemical model for a Li-ion cell using the local heat generation method and show simulations where significant 2D effects are seen. Subsequently, Gomadam *et al.*[16] use a similar approach and show the importance of a multidimensional model in describing cell behavior under certain conditions.

While these two classes of papers describe the development of thermal models where the heat generation term is estimated based on an electrochemical model, an alternate approach is to estimate this quantity based on experimental data. For example, Chen and Evans[1] use isothermal experimental discharge data, instead of an electrochemical model, to estimate heat generation rate and combine this with a thermal model for a cell stack. In other words, in their approach, the changes in the electrochemistry due to changes in the temperature of the cell are not addressed. However, this approach offers simplicity, as the solution to the electrochemical model with the associated coupled, nonlinear partial differential equations is not needed.

The goal of this paper is to gain insight into the coupling between the thermal and electrochemical behavior of Li-ion cells during operation by studying the behavior of a single cell. Specifically, we are interested in (*i*) examining the level of complexity needed to adequately describe the thermal-electrochemical behavior of cells; and (*ii*) gaining insight into the cause for the errors seen when making these approximations. These goals are achieved by performing various studies on a comprehensive 2D model based on a coupled thermal-electrochemical approach using the local heat generation method. These studies, which are performed under a wide range of operating conditions (*i.e.*, rates, thermal environment) and represented using summary plots, represents the novel contribution of this paper to the existing literature. In addition, the incorporation of recently presented data for the entropic heat in lithium manganese oxide spinel[5] and carbon,[6] as a function of SOC, makes this model

* Electrochemical Society Student Member.
** Electrochemical Society Active Member.
z E-mail: cxw31@psu.edu

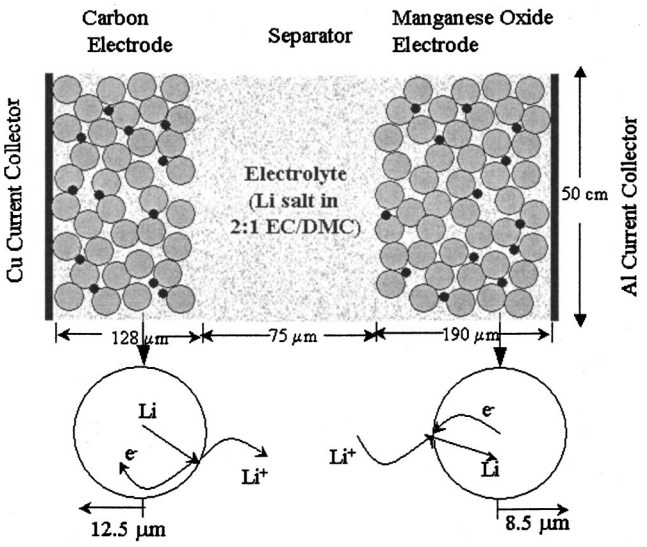

Figure 1. Schematic of the Li-ion cell used for this study (not to scale). The cell consists of a carbon negative, manganese spinel positive electrode with a separator between them with the cell filled with electrolyte. The electrochemical and thermal behavior is calculated from the model at each control volume in the cell in two dimensions.

more complex than others in the literature and thereby allows us to gauge the importance of this effect. The insight gained in this paper is expected to be used for development of a stack model where we wish to track the thermal and electrochemical behavior of each cell and study the way in which they interact with each other.

We begin by using the mathematical model to examine the need for a two-dimensional approach, and examine the interaction between the thermal behavior and the electrochemistry at different rates. In addition, the effect of the entropic heat term in the overall heat generation effect is quantified. Subsequently, considering the number of parameters that are known in the presently used model, we take the opportunity to reexamine the need for the local heat generation method in describing the behavior of the manganese oxide/carbon system and quantify the error in using the lumped thermal model as a function of rate. We also reexamine and quantify the approximation that heat generation data estimated under one thermal environment can be used to predict the behavior under other conditions, and provide insight into the differences by examining the changes in cell energy and utilization. The quantification of these two issues allows us to see if experimental voltage or calorimetric data, taken at specific conditions, can be used as a substitute for an electrochemical model in order to predict thermal excursions for the cell under study.

Mathematical Model

Electrochemical model.—The Li-ion cell modeled in this study, schematized in Fig. 1, consists of a Cu current collector, on which is pasted the carbon negative electrode, an Al current collector, on which is pasted the manganese oxide spinel, with a separator between the electrodes. The entire cell is filled with electrolyte, taken to be $LiPF_6$ in 2:1 ethylene carbonate (EC):dimethyl carbonate (DMC) in a poly(vinyl difluoride)-hexafluoropropylene (pVdf-HFP) matrix by virtue of the electrolyte parameter used. The cell represents a large electric vehicle (EV) battery with a considerably larger cell height compared to its thickness.[7] During charge/discharge, the reactions occurring in the two electrodes can be written as

$$\mathrm{Li}_{y-x}\mathrm{Mn_2O_4} + x\mathrm{Li}^+ + xe^- \underset{\text{charge}}{\overset{\text{discharge}}{\rightleftarrows}} \mathrm{Li}_y\mathrm{Mn_2O_4} \qquad [1]$$

$$\mathrm{Li}_x\mathrm{C_6} \underset{\text{charge}}{\overset{\text{discharge}}{\rightleftarrows}} \mathrm{LiC_6} + x\mathrm{Li}^+ + xe^- \qquad [2]$$

The electrochemical model equations are same as the one presented by Doyle *et al.*[17] and have been discussed by Gu and Wang[9] and hence are not described in detail here. The model uses porous electrode theory to address the porous nature of the electrodes and separator, concentrated solution theory for the mass balance and Ohm's law in the matrix, and a modified Ohm's law in solution to account for the charge balance.[18] In addition, the thermodynamics and kinetics of the charge/discharge reactions are also accounted for. The only difference between the model presented here and the one developed by Doyle *et al.*[17] is in the methodology by which the solid-state diffusion of Li into the active material is accounted for. While Doyle *et al.*[17] solve for Ficks law in spherical coordinates using the Duhamel's superposition principle to account for the time-dependent boundary condition,[14] we use the diffusion length approach, proposed by Wang *et al.*[19] Here the surface concentration is assumed to be related to the average concentration linearly at all times, which can be expressed as

$$\frac{D_s^{\mathrm{Li}}}{l_s}(c_s(t) - c_{\mathrm{avg}}(t)) = \frac{i(t)}{nF} \qquad [3]$$

where l_s is the diffusion length that can be estimated based on the geometry of the particles and is equal to $r_s/5$ for spherical particles. Note that Eq. 3 is valid only at long times when the diffusion length has reached a steady-state value. Empirical corrections to this term, of the form[20]

$$c_s(t) = c_{\mathrm{avg}}(t) + \frac{i(t)l_s}{nFD_s^{\mathrm{Li}}}[1 - e^{-4\sqrt{D_s^{\mathrm{Li}}t/3l_s}}] \qquad [4]$$

which incorporates another time-dependent term in an exponent similar to the time constant for diffusion, can be used to simulate short-time behavior.

All the parameters needed in the model, such as the concentration-dependent conductivity of the electrolyte, the OCP expression as a function of SOC, the exchange current density of the reactions, and transference numbers for the various species were taken from that of Doyle *et al.*[17] With the assumption that the current is assumed to be impressed through the tabs at the top of the cell (*i.e.*, flux of the potential is equated to a current at this boundary), the electrochemical profiles can be simulated in two dimensions and can result in the prediction of the overall cell voltage, potential in the matrix and solution phase, concentration variation in the cell, and the local SOC.[9]

Thermal model.—In order to simulate the thermal excursions in the cell, this electrochemical model is combined with an energy balance, namely[11,21]

$$\frac{\partial(\rho C_p T)}{\partial t} = \nabla \cdot (\lambda \nabla T) + q \qquad [5]$$

which accounts for heat accumulation, conduction, and generation in each control volume across the cell based on the local heat generation method. Assuming a binary electrolyte and neglecting the enthalpy of mixing and phase change effects, the heat generation term can be estimated based on the various losses in the cell, and expressed as[9,11,21]

$$q = \sum_j a_{sj} i_{nj}(\phi_s - \phi_e - U_j) + \sum_j a_{sj} i_{nj} T \frac{\partial U_j}{\partial T} + \sigma^{\mathrm{eff}} \nabla\phi_s \cdot \nabla\phi_s + \kappa^{\mathrm{eff}} \nabla\phi_e \cdot \nabla\phi_e + \kappa_D^{\mathrm{eff}} \nabla \ln c_e \cdot \nabla\phi_e \qquad [6]$$

where the summation is over all reactions. The first term on the right represents the deviation of the potential in each control volume from

Table I. The parameters used to generate the model simulations are listed here. All, except the initial SOC and the initial electrolyte concentration, are transposed from Ref. 9.

Quantity	Unit	Value				
		Cu	Anode	Separator	Cathode	Al
Thickness	μm	10	128	76	190	15
Density	g/cm^3	9.0	2.5	1.2	1.5	2.7
Specific heat	J/g K	0.381	0.7	0.7	0.7	0.87
Thermal conductivity	W/cm K	3.8	0.05	0.01	0.05	2.0
Particle radius	μm		12.5		8.5	
Initial SOC			0.7		0.15	
Maximum concentration in solid phase	mol/cm^3		0.02639		0.02286	
Diffusion coefficient-solid phase	cm^2/s		3.9×10^{-10}		1×10^{-10}	
Exchange current density	A/cm^2		0.11×10^{-3}		0.08×10^{-3}	
α			0.5		0.5	
Diffusion coefficient-electrolyte	cm^2/s			7.5×10^{-7}		
Transference number				0.363		
Initial electrolyte concentration	mol/cm^3			1×10^{-3}		
Activation energies						
Exchange current density	kJ/mol		30		30	
Diffusion coefficient-solid	kJ/mol		4		20	
Diffusion coefficient-liquid	kJ/mol			10		
Electrolyte conductivity	kJ/mol			20		

the equilibrium potential (termed irreversible heat in this paper). The second term arises from the entropic effect (reversible heat). Summation of the two terms accounts for the irreversible and reversible heats associated with each electrochemical reaction. The third term represents the ohmic heat arising from the matrix phase, while the last two terms arise from ohmic heats in the solution phase. Note that all the terms that are needed in Eq. 6 are predicted using an electrochemical model, hence allowing us to simulate the thermal-electrochemical behavior of the cell. However, as the temperature of the cell changes, the various controlling parameters in Eq. 6, like diffusion coefficients and conductivities, change. These are estimated based on Arrhenius-type relations, similar to those used by Botte *et al.*[8] Note that Eq. 6 would be different if the film resistance, caused by the SEI layer, were also included, with modification of the overpotential term in the kinetic expression.[17] This would cause an added heating effect in the cell. In this study, the film resistance was assumed to be zero. All thermal parameters used in this study are taken to be the same as that in Ref. 9. The relevant parameters are transposed for convenience in Table I.

Recent experimental measurements of the reversible heat on both the carbon and the $LiMn_2O_4$ electrodes has provided us with a means of simulating this feature. For the manganese oxide spinel, the data reported by Thomas *et al.*[5] was fit to an empirical equation of the form

$$\frac{dU}{dT} = 4.31274309\exp(0.571536523y) + 1.281681122\sin(-4.9916739y) - 0.090453431\sin(-20.9669665y + 12.5788250) - 0.0313472974\sin(31.7663338y - 22.4295664) - 4.14532933 + 8.147113434y - 26.064581y^2 + 12.7660158y^3 - 0.184274863\exp\left(-\frac{y - 0.5169435168}{0.04628266783}\right)^2 \quad [7]$$

while for the carbon electrode the data from Al Hallaj *et al.*[6] where the dU/dT was reported as a function of voltage was converted to that of SOC using the equilibrium potential *vs.* SOC correlation from Doyle *et al.*[17] to yield

$$\frac{dU}{dT} = 344.1347148 \times \frac{\exp(-32.9633287x + 8.316711484)}{1 + 749.0756003\exp(-34.79099646x + 8.887143624)} - 0.8520278805x + 0.362299229x^2 + 0.2698001697 \quad [8]$$

It should be noted that the entropy measurement was performed on a graphitic carbon electrode, which has been assumed to be representative of the carbon electrode in this paper. However, there may exist differences between the two carbons, considering the physical significance of the entropy change with SOC.[5] The fits of these equations to the experimental data are shown in Fig. 2. While the data on $LiMn_2O_4$ is substantial, that on the carbon electrode is concentrated on the intermediate SOC and hence is unreliable at the beginning and end of discharge. Caution needs to be exercised in using Eq. 6 along with the entropic correlations, because of the implicit assumption that the entropy does not vary with temperature

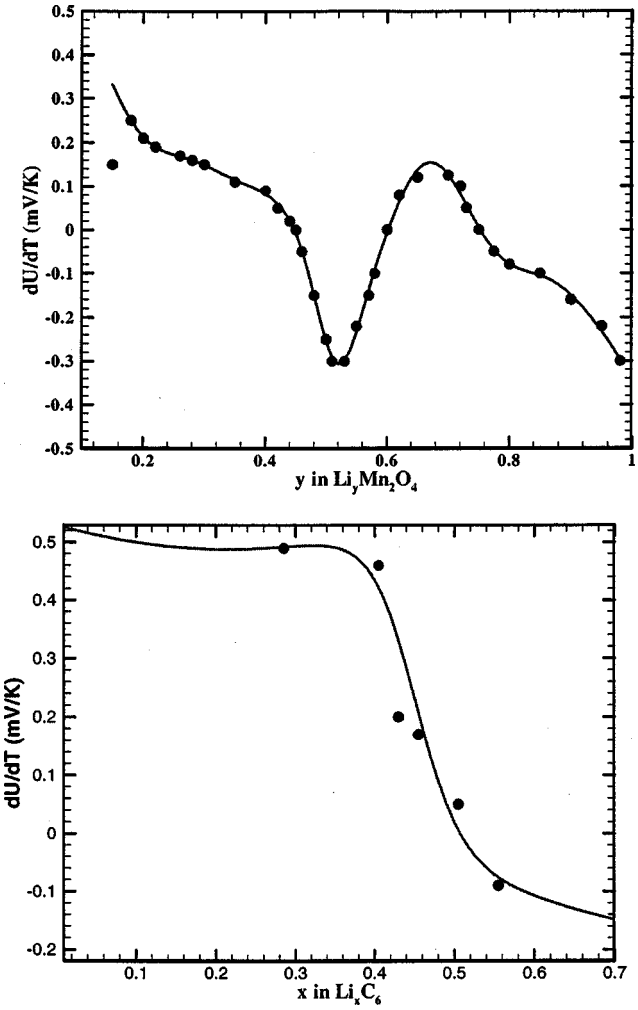

Figure 2. Experimentally determined entropic heat as a function of SOC for the manganese spinel (top) and carbon (bottom) electrodes taken from Ref. 5 and 6, respectively. The plots also show the fit obtained using Eq. 7 (top) and 8 (bottom).

(the temperature at which the entropy measurements were performed is different from those accessed in this paper). In addition, a temperature distribution across the thickness of the cell would lead to ambiguities in relating the two different entropic terms for the two electrodes, due to the differences that would exist for the temperature of the counter electrode with which the measurement was performed. As the temperature variation across the cell thickness is negligibly small in all the simulations shown in this paper, any errors resulting from this are expected to be minimal.[18,22] However, as temperature gradients exist in the vertical dimension of the cell, and as current is passing in this direction, additional thermoelectric effects could emerge in this direction.

The electrochemical and thermal model equations were solved simultaneously by first descretizing them using a control volume formulation after which the equations are solved using a Newton's method. The resulting Jacobian matrix is solved iteratively using a GMRES subroutine in conjunction with Gauss-Seidal and Multigrid preconditioners.[23] A typical discharge of the cell is simulated in less than 10 min using this numerical recipe.

Results and Discussion

All results are shown during discharge of a 2.9 Ah Li-ion cell, whose cell dimensions are represented in Fig. 1. All parameters (cell specific, thermodynamic, etc.) are based on Ref. 7 and 17 and are summarized in Ref. 9. The capacity of the cell is defined using the maximum concentration of dischargeable lithium, which is calculated from the initial stoichiometry of the two electrodes (0.7 for carbon and 0.15 for manganese, during discharge) and the maximum concentration of lithium in the lattice.[17] The smaller of the two numbers is the capacity of the cell and corresponds to that of the manganese oxide cathode, in order to prevent Li deposition in the anode on overcharge. The SOC of the cell is defined as the ratio of the discharged capacity to the cell capacity.

Figure 3 details (a) 2D temperature and (b) reaction current contours generated using the model at a discharge rate of 2 C at 50% SOC. The cell was simulated under nonisothermal conditions where infinite heat-transfer was assumed to occur from the top of the cell while no heat-transfer occurs from the sides and the bottom. This can be thought of as the center cell in a large EV cell stack where cooling is provided only through the tabs with adiabatic conditions on the sides. Due to the large aspect ratio (cell height to cell thickness), considerable differences are seen in the temperature between the bottom and the top of the cell with differences as large as 35°C, with a much smaller temperature at the cell top owing to the transfer of heat to the ambient, which is maintained at 25°C. Figure 3 suggests that under certain conditions a 2D thermal model is necessary. It should be noted that for cells with a smaller aspect ratio or when the thickness of the current collectors (which have two orders of magnitude larger thermal conductivity) is increased, the temperature variation decreases considerably, reducing the need for a 2D model.

The difference in temperature across the cell height results in differences in the electrochemistry as seen from Fig. 3b, which shows the reaction current distribution corresponding to the temperature profile in (a). Even under isothermal conditions, considerable differences in reaction current are expected at different points in the cell depending on the ratio of the matrix to solution conductivity, the kinetic resistance, and the slope of the equilibrium potential *vs.* SOC curve.[24] These differences are seen across the thickness of the cell, at the bottom, where the temperature is uniform. These are amplified when the temperature variations are superimposed. This can be seen clearly in the carbon electrode where the reaction current changes with cell height, at the top of the cell, corresponding to the change in temperature.

This change in the electrochemical behavior with temperature occurs not only in the internal profiles of the cell, as shown in Fig. 3, but is also reflected in the cell voltage as seen in Fig. 4. Here the voltage of the cell is plotted *vs.* depth of discharge (DOD) under isothermal and nonisothermal (infinite heat-transfer from the tabs) conditions at different C-rates. All isothermal simulations in the paper were conducted at room temperature (25°C). At low rates (0.01 C) the cell is practically at equilibrium and all the heat generation occurs due to the reversible heat. In addition, the large time of discharge ensures that the heat generated is dissipated from the cell even when heat-transfer occurs only from the top of the cell. As the temperature rise is small, no change is seen in the electrochemical behavior and the isothermal and nonisothermal voltage curves coincide.

However as the rate of discharge increases, the cell starts to deviate from equilibrium and hence heat generation starts to increase, and the cell temperature (illustrated in Fig. 5 and 6) increases. This increase is further enhanced due to the short time for the heat to dissipate when compared to the lower discharge rates. The increase in cell temperature in turn results in a decrease in the ohmic, kinetic, and mass-transfer losses in the cell; hence, the overall cell voltage starts to increase as seen from the solid line in Fig. 4, when compared to the isothermal curves (dotted line). In addition, the mass-transfer rates, both in the solid and liquid phases, increase, thereby resulting in an increase in the utilization of the cell. For example, at a discharge rate of 2 C the utilization increases from 50 to 75%, resulting in considerable improvement in the performance of the cell. However, this increase is at the risk of increasing the temperature, with the ensuing unsafe operation.

This increase in temperature is seen in Fig. 5, where the evolution is shown during discharge at 2 C. The monotonous increase to

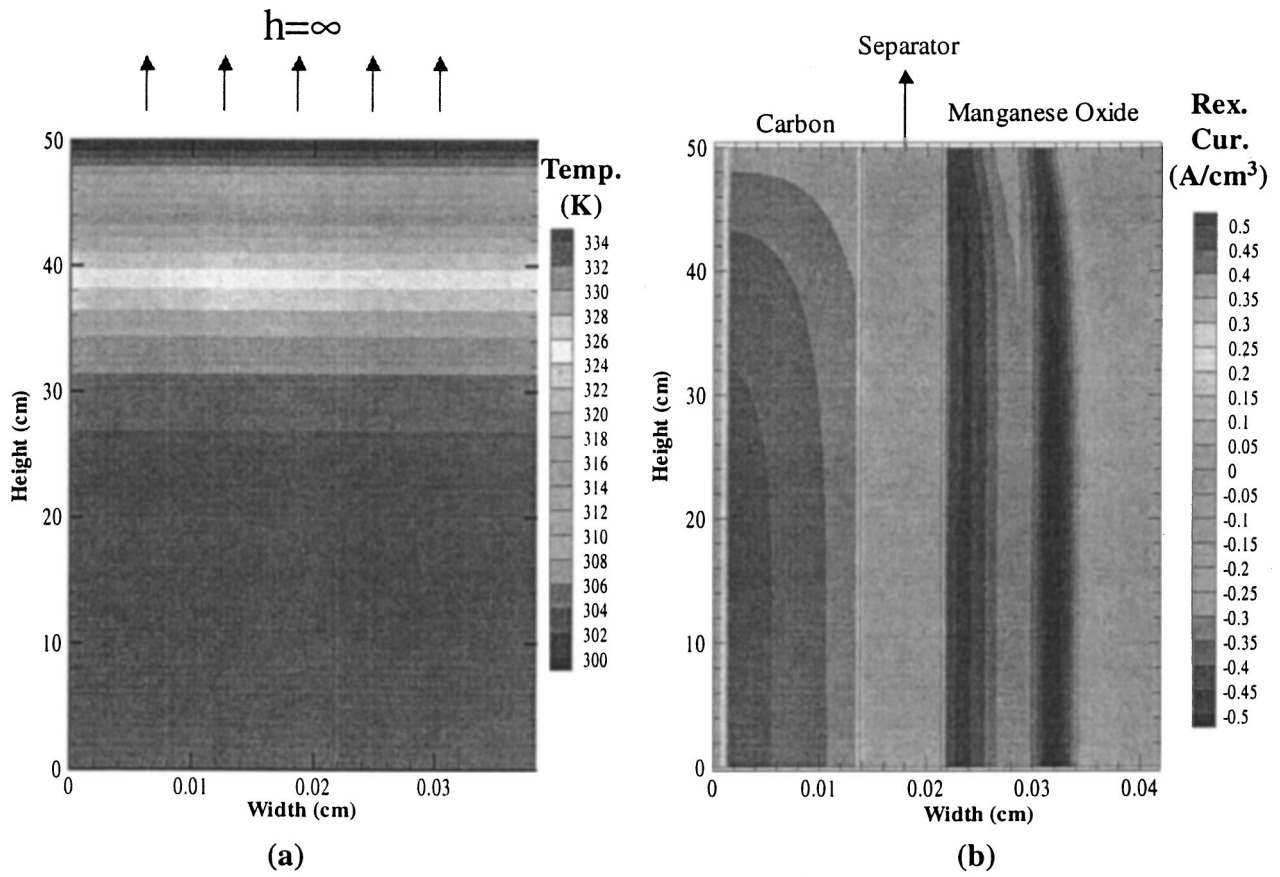

Figure 3. Temperature (left) and reaction current (right) distributions in the cell during constant current discharge at a rate of 2 C generated using the 2D thermal-electrochemical model. While the top of the cell is assumed to have infinite heat-transfer, the other three sides are maintained under adiabatic conditions. Note the change in reaction distribution both across and with increasing height in the cell.

80°C by the end of discharge asserts to the need for a thermal management system in Li-ion cells. The significant deviation of the cell from its equilibrium is clearly seen in this figure from the contributions of the different terms in Eq. 6 toward the temperature increase in the cell. The large electronic conductivity of the solid phases results in the ohmic heat in the matrix phase being negligible. However, the ohmic heat in the solution, reversible and irreversible heats, all contribute significantly to the overall heat generation in the cell. While the reversible heat is negative at the beginning of discharge and then changes sign as discharge proceeds (as dictated by the nature of the dU/dT *vs.* SOC curves), the other heats are positive and thereby exothermic. However, as the total heat generated is exothermic all through the discharge, the temperature rises monoto-

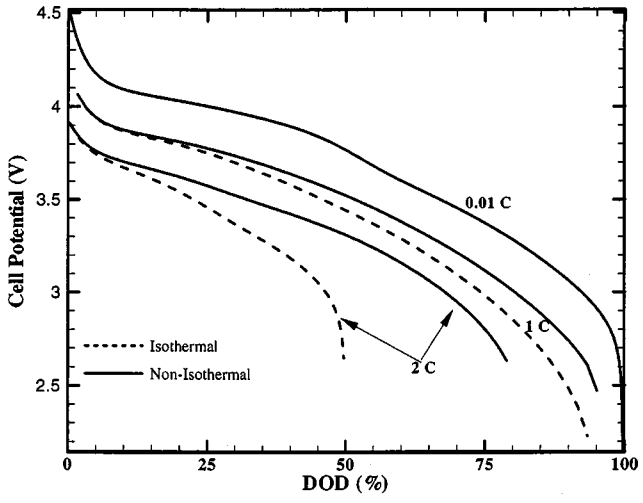

Figure 4. Simulated (— — —) isothermal and (——) nonisothermal discharge curves under different rates. The nonisothermal case was simulated with infinite heat-transfer from the tabs and adiabatic conditions on the other three sides.

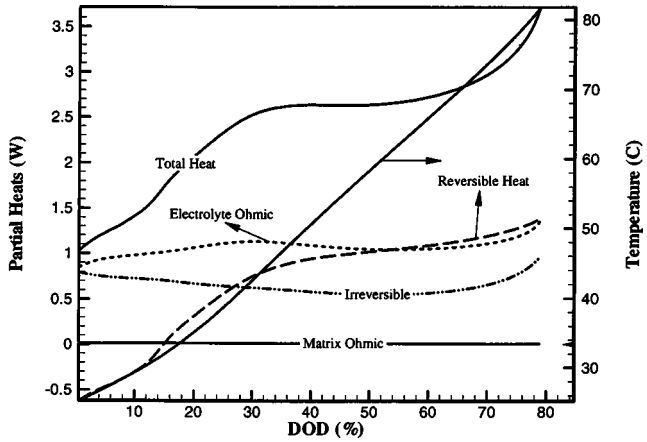

Figure 5. Partial heats due to the various sources contributing to the total heat in the cell during a simulated 2 C discharge of a Li-ion cell. Also shown is the temperature rise in the cell.

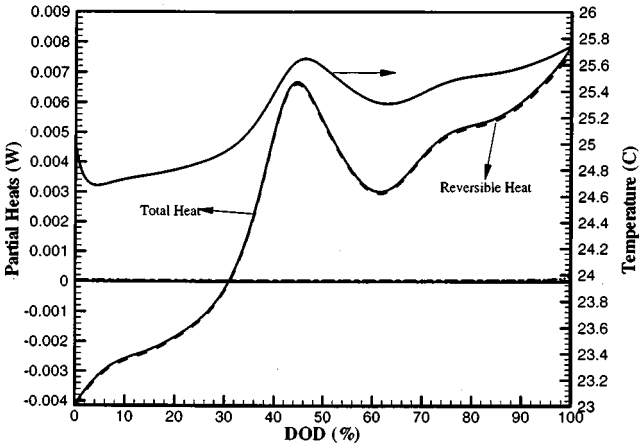

Figure 6. Partial heats due to the various sources contributing to the total heat in the cell during a simulated 0.01 C discharge of a Li-ion cell. Also shown is the temperature rise in the cell. Note the bumps in the temperature and heat profiles.

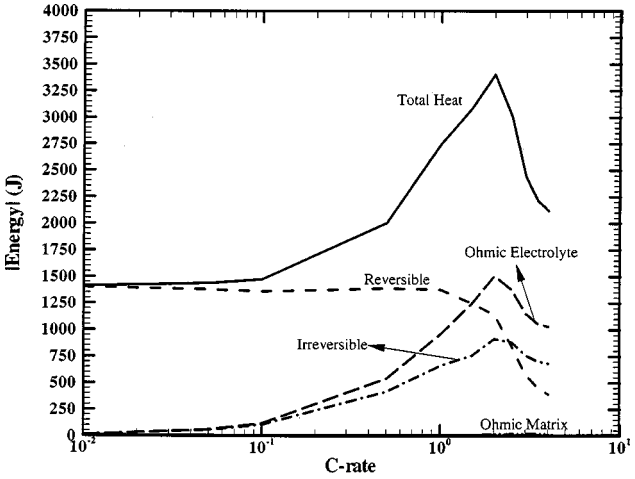

Figure 7. The partial thermal energy contributing to the total energy generated through discharge at various C rates. The curves were generated by estimating the area under the heat-time curves (similar to Fig. 5 and 6) by taking the modulus of the heat values.

nously. Figure 5 illustrates that the reversible heat is important in $LiMn_2O_4$/carbon cells even when the rate of discharge is fairly large.

When the rate of discharge is now decreased so as to approach equilibrium, the importance of the reversible heat is further exemplified, as seen in Fig. 6. Under these conditions, although the temperature rise is negligible, all heat generation is due to the reversible heat effects, seen from the closeness of the dotted line (reversible heat) to the solid line (total heat). Therefore, the temperature profile shows a decrease, corresponding to the endothermic part of the reversible heat, after which the temperature starts to rise. In addition, the temperature rise is not monotonous, as seen in Fig. 5, but displays bumps, in accordance with the profiles seen in the dU/dT *vs.* SOC curves. Combined with this effect is the heat dissipation to the external ambient which influences the nature of these curves significantly, considering the long time of discharge. This external heat transfer results in the cell temperature increasing to reach the ambient at the beginning of discharge (after the initial decrease), although the cell behaves endothermically. Such heat generation curves, with endothermic regions at the start of discharge and exothermic regions through the rest, with bumps at intermediate DODs, have been seen experimentally.[3] A more detailed quantitative comparison is not possible at this time, considering that many of the device-specific quantities needed for the model are not known for the cell studied experimentally. In addition, a true comparison can only be made when more comprehensive data for the entropy of the carbon electrode is used. In summary, Fig. 5 and 6 show that the reversible heat is an important effect that needs to be included in models for Li-ion cells.[25] However, the relative importance of this effect is different depending on the discharge rate.

In order to summarize these effects and capture this rate-dependent contribution of the various heats in the cell, the area under the heat *vs.* DOD curve was plotted at various C-rates, as shown in Fig. 7. However, as the reversible heat has both exothermic and endothermic parts at different DODs, this approach can lead to underestimation of this effect. For example, in Fig. 6, if the discharge is cut-off at 50% DOD, the reversible heat contribution would cancel out, although the profile is completely dictated by this term. Therefore, the plots were made by taking the absolute values of the partial and total heats, whereby even partial discharges would be adequately represented. However, the effect of performing this was seen to be negligible when compared to curves without this conversion, especially at higher rates.

The resulting plot, seen in Fig. 7, shows that irrespective of the rate, the ohmic heat in the matrix is negligible considering its large conductivity. At low rates, all the heat is primarily due to entropic effects. As the rate is increased, the irreversible and ohmic heat in the electrolyte also start to increase, in correlation with the increasing losses in the cell. This increase also results in the total heat increasing. Note that such an increase is not seen in the reversible heat, with the energy remaining constant as the rate is increased, as this is a thermodynamic and hence a rate-independent quantity. Figure 7 shows that irrespective of the rate, the reversible heat is an important contribution, indicating that mathematical models need to consider this effect.

As the rate is increased further, the energy decreases for all the curves, which results in a peak in all but the reversible heat. This decrease is a consequence of the decreasing utilization in the cell, resulting in less time of discharge. As the discharge time decreases, the time for heat generation decreases and hence the total energy decreases. Although the heat generated is large at high rates, this decrease in discharge time results in a decrease in the total heat generated in the cell. In summary, the effects seen in Fig. 7 are a consequence of the increasing inefficiencies in the cell, asserting to the need for an electrochemical model to predict the heat generation.

These inefficiencies can be captured by tracking the area under the voltage *vs.* time curve (*i.e.*, the electrical energy) and the utilization at the various rates, as shown in Fig. 8. At low rates both the electrical energy and the utilization remains at the maximum and hence all the heat generated is due to the entropic effect. As the rate is increased, the energy starts to decrease due to the decreasing cell voltage caused by ohmic, kinetic, and mass-transfer losses. This results in the increase in heat generation shown in Fig. 7. Further increase in the rate results in a drastic decrease in the utilization of the cell with the ensuing decrease in the electrical energy, which results in the peak. Note that the nature of the curve shown in Fig. 8 and hence the results shown in Fig. 7 depend on the design of the cell. For example, a decrease in the particle size would result in higher utilization at the same rate, thereby pushing the peak, seen in Fig. 7, to a higher rate. In contrast, making the electrodes and separator thinner (thin-film batteries) would reduce ohmic losses and hence decrease the magnitude of the total heat generated, while keeping the position of the peak the same. Thus, a detailed quantitative prediction of the behavior of a real cell would be possible only by performing extensive model-experimental comparisons.

This decrease in utilization and the ensuing decrease in the thermal energy also results in a peak in temperature, as seen in Fig. 9. Here the average cell temperature at the end of discharge is plotted with C rate. In addition to the inefficiencies in the cell, the temperature is also effected by the time of discharge, as heat is dissipated from the tabs during this time. This effect is the cause for the neg-

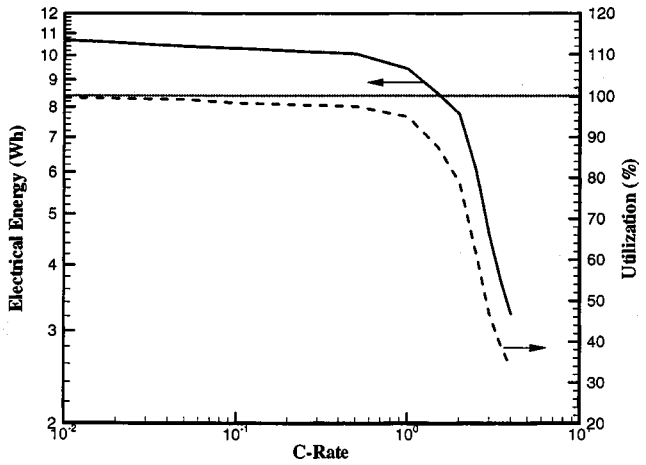

Figure 8. Simulated electrical energy and utilization at various C rates during discharge of the Li-ion cell. The deviation in the electrical energy from its maximum value results in heat generation. The drop in utilization results in a decrease in the time for heat generation and is the cause for the peak seen in Fig. 7.

ligible temperature increase seen in Fig. 9 at low rates, although the entropic effect results in heat generation (solid line). If the cell were operated adiabatically, the temperature would be higher. However, as the rate is increased, the inefficiencies increase, resulting in more heat generation. This, combined with the decreasing time of discharge, results in the increase in the final temperature. Finally, as the utilization decreases, the heat generation decreases and hence the final temperature decreases, resulting in a peak.

Figure 9 also illustrates the importance of entropic heat in accurately predicting cell temperature. The significant difference between the solid and the dotted lines shows a need to include this effect at higher rates, while its contribution is negligible at low rates. However, note that the negligible contribution at low rates is caused by the fact that the cell is operated under nonisothermal conditions whereby the heat is dissipated through the tabs. If the cell were operated adiabatically, then the difference between the dotted and solid lines would be relatively constant, as dictated by the relatively constant contribution of the entropic heat term in Fig. 7, prior to the

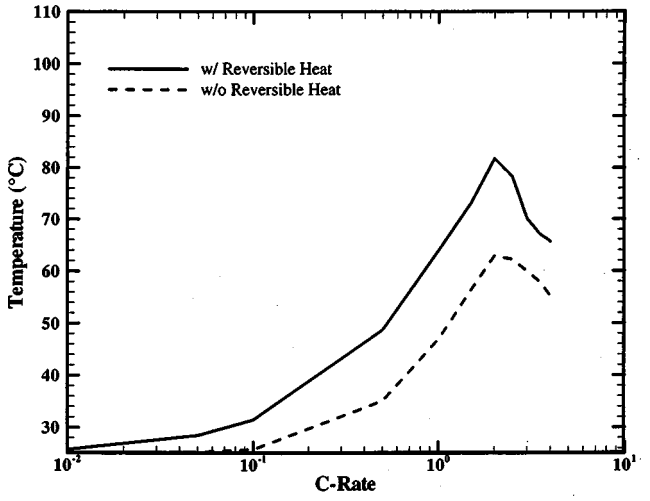

Figure 9. Simulated temperature rise at various C rates during discharge of a Li-ion cell. The plot quantifies the effect of adding the reversible heat on the temperature at the end of discharge. Note that the difference in temperature between the two curves changes with C rate due to the differing time for heat dissipation.

point of decreased utilization. In summary, Fig. 3–9 assert that while the thermal behavior of the cell is dictated by the electrochemistry, the electrochemical behavior is affected significantly by the thermal excursions. The coupling of the two gives rise to thermal runaway.[26]

This illustrates the use of a thermal model (Eq. 4) where the heat generation is estimated from an electrochemical model, thereby resulting in considerable complexity. One could attempt to simplify this approach by using a thermal model along with experimental data for the heat generation. This is achieved by first performing a lumped thermal model over the entire cell. Under conditions where the temperature is uniform all over the cell (small Biot number), Eq. 4 can be substituted with[11,15,21]

$$\frac{d(\rho_{avg}C_{p,avg}T_{avg})}{dt} + \frac{hA(T_{avg} - T_{amb})}{V_c} = \langle q \rangle \qquad [9]$$

where the heat generation term is obtained by integrating Eq. 6 over the whole cell to yield

$$\langle q \rangle = \frac{1}{V_c}\int_{V_c} q dv \qquad [10]$$

Under conditions where the reaction distribution is uniform across the entire porous electrode and when no side reactions are present, Eq. 9 is simplified to yield the expression derived by Bernardi *et al.*[15]

$$\langle q \rangle = I\left(U_{avg} - V_{cell} - T_{avg}\frac{\partial U_{avg}}{\partial T_{avg}}\right) \qquad [11]$$

Therefore, experimental discharge (or charge) curves can be used to estimate the heat generation rate based on the measured cell potential at a particular current, in conjunction with the equilibrium potential *vs.* SOC and the entropy *vs.* SOC curves.[1] Experiments are conducted under a controlled thermal environment (say isothermal) and the results used to predict heat generation at all other conditions. In order for this approach to accurately predict the thermal behavior of the cell, three assumptions have been implicitly made, namely, (i) that the temperature profile in the cell is uniform;[11] (ii) the heat generation estimated from Eq. 11 is the same as that from Eq. 6, or in other words, the reaction current distribution in the porous electrode is uniform,[11] and (iii) heat generation rates estimated under a particular thermal environment can be used to adequately estimate the heat generation in other environments.[13] While assumption (i) may be acceptable for cells that are shorter than those used in this study, (ii) and (iii) are questionable and are explored in this paper for the cell under study. An alternative approach to using experimental voltage data is to measure heat generation directly (*e.g.*, using either an isothermal or an adiabatic calorimeter) and eliminate the need for Eq. 11 and the associated assumption (ii). However, this approach still depends on the validity of assumption (iii).

Figure 10 explores the difference between the thermal energy estimated from the local heat generation method and that from Eq. 10, under isothermal conditions. The latter was determined from the model by estimating the average SOC of each electrode and estimating the equilibrium potential and the entropy term at this average value. In other words, this approach explores the assumption of uniform reaction distribution in the electrodes. For example, when the reaction is uniform, the average SOC and the local SOC would be the same, and hence both methods would yield the same value. Such a scenario occurs when the discharge rate is small and the resulting similarity is seen in Fig. 10 at the low C-rates. However, as the rate of discharge increases, the nonuniformity (illustrated in Fig. 3b) increases and the two plots start to deviate from each other with as much as 15% difference between the two with the lumped model overestimating the heat at all C rates. Figure 10 clearly suggests that assumption (ii) is valid only under low discharge rates and is not appropriate at higher rates. In addition to differences in the overall

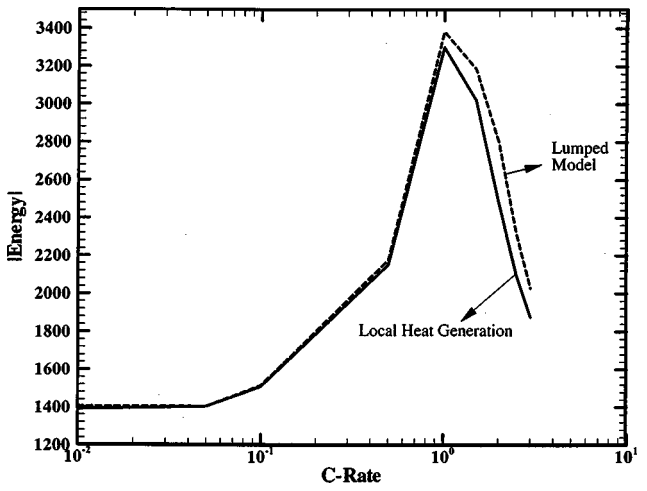

Figure 10. Comparison of the thermal energy generated using the local heat generation and the lumped thermal models under adiabatic conditions. The plot is a consequence of the nonuniform reaction distribution in the porous electrodes. While at low rates these effects are negligible, higher rates results in the effects becoming more predominant.

heat generation, differences are also seen in the evolution of the profile during the discharge.[11] Therefore, estimation of heat generation data directly is preferable to using voltage information in order to accurately predict the temperature rise under a given thermal environment.

However, even if the heat generation data is measured directly, assumption (*iii*), where the heat generation rate is assumed to be independent of the thermal environment also needs to be valid. Considering the intimate relationship between the temperature of the cell and the heat generation rate, this assumption is highly questionable. This is clearly seen in Fig. 11, where the thermal energy is plotted with C rate under isothermal and adiabatic conditions is compared to that shown in Fig. 7, when heat transfer occurs from the tabs. At low rates, when the temperature rise is small, little difference is seen in the three cases, suggesting that the assumption is valid. However, as the rate increases and the temperature starts to increase, the electrochemical behavior is modified by the temperature change, which is turn affects the heat generation rate. This relationship can be better understood by looking at Fig. 11 in tandem with Fig. 12a and b, which shows the electrical energy (area under the voltage *vs.* time curve) and the utilization of the cell, respectively.

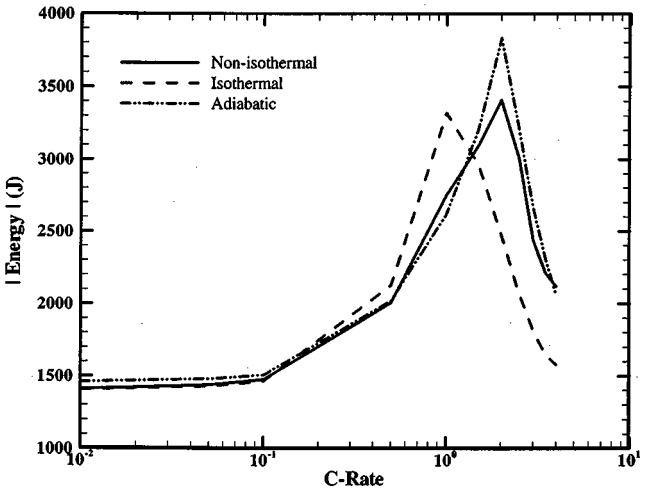

Figure 11. Simulated thermal energy as a function of C rate under adiabatic, isothermal, and nonisothermal conditions. The nonisothermal case is same as the one shown in Fig. 7 and corresponds to infinite heat transfer from the tabs with adiabatic conditions on the other three sides of the cell. Note that each curve has a different heat generation rate, suggesting that heat generation rate under one thermal environment cannot be used to simulate behavior under other conditions.

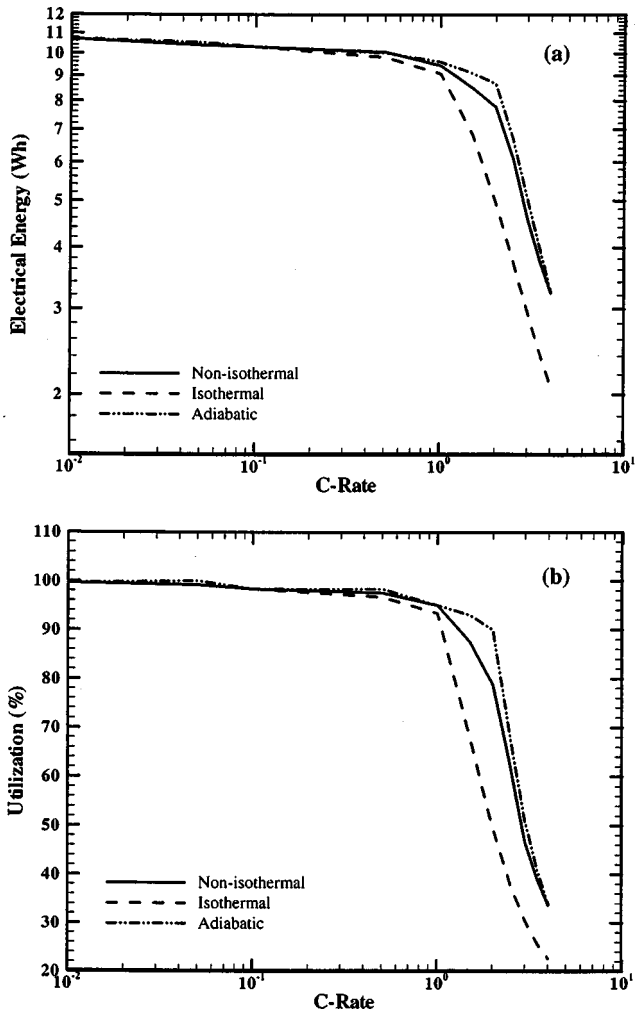

Figure 12. Simulated (top) electrical energy and (bottom) utilization *vs.* C rate under adiabatic, isothermal, and nonisothermal conditions. The combined effect of the two quantities results in the nature of the curves seen in Fig. 11.

When operating the cell under isothermal conditions, the increase in efficiency as the temperature increases does not occur, as seen by comparing the electrical energy curves between the isothermal and the nonisothermal cases. This leads to greater heat generation at lower rates under isothermal conditions as seen in Fig. 11. However, as the rate is increased further, the lower temperature results in an increased diffusion limitation in the cell, which in turn results in lowered utilization, leading to the occurrence of the peak in the thermal energy at a lower C rate. Beyond this point, the isothermal heat generation is lower than that predicted from the nonisothermal operation. Overall as much as 40% difference is seen between the two curves.

While isothermal conditions show differences in the C rate at which the peak is formed and in the actual values of the heat generation rate, adiabatic conditions do not show this deviation in the peak position. When the cell is operated under adiabatic conditions, the temperature rise is larger than that under nonisothermal conditions and hence the efficiency is even larger. This results in a slightly lesser heat generation rate under this condition, as seen in Fig. 11. However, as the C rate increases, the utilization of the cell under

adiabatic conditions is larger than that under nonisothermal conditions (Fig. 12b) and hence results in longer time for heat generation, although the efficiency of the process is larger (Fig. 12a). This increased time for heat generation results in larger heat generation under adiabatic conditions compared to the other two. Therefore, the heat generated under adiabatic conditions, while being similar to the nonisothermal conditions under most C rates, deviates significantly around the peak position.

Figure 11 and 12 illustrate the intimate relationship between the heat generation and the thermal and electrochemical conditions in the cell and asserts to the fact that heat generation under any one condition cannot be used to simulate those under other conditions. While the curves under nonisothermal and isothermal conditions appear to be similar through most C rates in Fig. 11, a different cell design with differences in the utilization and efficiency could result in different results from what is shown here. In addition, the significant differences between the isothermal and the nonisothermal cases could become less as the temperature under which the isothermal cell is operated becomes higher than room temperature; again pointing to the need for a model-based approach.

Conclusions

A 2D, coupled, thermal-electrochemical modeling study for a manganese oxide spinel/carbon cell based on the local heat generation method has been presented. The model incorporates the reversible, irreversible, and ohmic heats in the matrix and solution phases. The temperature coefficients of the various transport and kinetic parameters are accounted for using Arrhenuis-type relationships based on the literature data. In addition, recently published experimental data on the entropic heat for the manganese oxide and the carbon electrode as a function of SOC are included.

Model simulations were first used to show the 2D effects that can occur in cells with a large aspect ratio, under certain conditions. Subsequently, simulations conducted at different rates were used to gauge the importance of the various contributions to the total heat generated in the cell. The reversible heat was found to be important at all rates and was seen to contribute both to the final temperature of the cell at all rates and to the evolution of the temperature during discharge, especially at low rates. Model simulations, used to estimate the thermal and electrical energy and the utilization of the cell at various rates, were used to gain insight into the effect of the electrochemistry on the heat-generation and vice versa.

The model was also used to test the hypothesis of using experimental voltage or calorimetric data to estimate the heat generation under one thermal environment, which is then used to predict heat generation under other environments. It was shown that the nonuniform reaction distribution in the porous electrode was significant at higher rates, which in turn introduces error in estimating the heat generation based on the average cell voltage and open-circuit voltage, with as much as 15% difference between the two methods. Therefore, the use of voltage data to estimate heat generation was shown to be less rigorous compared to measuring this quantity directly from calorimetric data. However, even the latter approach needs to be used with caution as the heat generation measured under one thermal environment (say isothermal) cannot be used under any other conditions. While at low rates the differences were negligible, significant deviations (as much as 40%) were seen when using this approach at higher rates.

Acknowledgments

The authors are grateful to Dr. Wen-Bin Gu (GM Global Alternative Propulsion Center) for developing the model and Dr. J. Wu (Department of Mathematics, Penn State University) for developing the solution procedure. This work was supported, in part, by the DOT Advanced Vehicle Program under cooperative agreement no. DTRS56-99-T-0016.

The Pennsylvania State University assisted in meeting the publication costs of this article.

References

1. Y. Chen and J. Evans, *J. Electrochem. Soc.*, **143**, 2708 (1996).
2. J. Hong, H. Maleki, S. Al Hallaj, L. Redey, and J. R. Selman, *J. Electrochem. Soc.*, **145**, 1489 (1998).
3. J. Kim, J. Prakash, and J. R. Selman, *Electrochem. Solid-State Lett.*, **4**, A141 (2001).
4. E. P. Roth, Abstract 163, The Electrochemical Society Meeting Abstracts, Vol. 2000-2, Phoenix, AZ, Oct 22-27, 2000.
5. K. Thomas, C. Boguta, and J. Newman, *J. Electrochem. Soc.*, **148**, A570 (2001).
6. S. Al Hallaj, R. Venkatachalapathy, J. Prakash, and J. R. Selman, *J. Electrochem. Soc.*, **147**, 2432 (2000).
7. D. Baker and M. Verbrugge, *J. Electrochem. Soc.*, **146**, 2413 (1999).
8. G. Botte, B. Johnson, and R. White, *J. Electrochem. Soc.*, **146**, 914 (1999).
9. W. B. Gu and C. Y. Wang, in *Lithium Batteries*, S. Surampudi, R. A. Marsh, Z. Ogumi, and J. Prakash, Editors, PV 99-25, p. 748, The Electrochemical Society Proceedings Series, Pennington, NJ (2000).
10. C. Pals and J. Newman, *J. Electrochem. Soc.*, **142**, 3274 (1995).
11. L. Rao and J. Newman, *J. Electrochem. Soc.*, **144**, 2697 (1997).
12. L. Song and J. W. Evans, *J. Electrochem. Soc.*, **147**, 2086 (2000).
13. C. Pals and J. Newman, *J. Electrochem. Soc.*, **142**, 3282 (1995).
14. M. Doyle, T. F. Fuller, and J. Newman, *J. Electrochem. Soc.*, **140**, 1526 (1993).
15. D. Bernardi, E. Pawlikowski, and J. Newman, *J. Electrochem. Soc.*, **132**, 5 (1985).
16. P. M. Gomadam, J. W. Weidner, and R. E. White, Abstract 52, The Electrochemical Society Meeting Abstracts, Vol. 2001-1, Washington, DC, March 25-30, 2001.
17. M. Doyle, J. Newman, A. S. Gozdz, C. N. Schmutz, and J. Tarascon, *J. Electrochem. Soc.*, **143**, 1890 (1996).
18. J. Newman, *Electrochemical Systems*, 2nd ed., Prentice-Hall, Inc., Englewood Cliffs, NJ (1973).
19. C. Y. Wang, W. B. Gu, and B. Y. Liaw, *J. Electrochem. Soc.*, **145**, 3407 (1998).
20. C. Y. Wang and V. Srinivasan, *J. Power Sources*, In Press.
21. W. B. Gu and C. Y. Wang, *J. Electrochem. Soc.*, **147**, 2910 (2000).
22. J. Newman, *Ind. Eng. Chem. Res.*, **34**, 3208 (1995).
23. J. Wu, V. Srinivasan, J. Xu, and C. Y. Wang, *J. Electrochem. Soc.*, **149**, A1342 (2002).
24. T. Fuller, M. Doyle, and J. Newman, *J. Electrochem. Soc.*, **141**, 1 (1994).
25. K. E. Thomas and J. Newman, *Intercalation Compounds for Battery Materials*, G. A. Nazri, T. Ohzuku, and M. Thackeray, Editors, PV 99-24, p. 370, The Electrochemical Society Proceedings Series, Pennington, NJ (1999).
26. M. W. Verbrugee, *AIChE J.*, **41**, 1550 (1995).